

Photoelectrochemically-Induced Gold Deposition on p-GaAs Electrodes

Part II. Size Effects in Photoselective Patterning

Jan W. M. Jacobs and Jan M. G. Rikken

Philips Research Laboratories, 5600 JA Eindhoven, The Netherlands

ABSTRACT

Circular Au spots with radii ranging from 5 to 250 μm were photocathodically deposited from an alkaline $\text{KAu}(\text{CN})_2$ solution with excess CN^- ions on low-doped p-GaAs disk electrodes with diameters ranging from 10 μm to 8 mm. It is shown that illuminated spots on the p-GaAs substrate behave as microdisk electrodes at which the supply of reactants is enhanced by spherical diffusion. The dissolution kinetics of deposited Au spots after illumination and the possibility of electroless gold deposition on the Au spots are discussed. Both are determined by the open-circuit potential of the electrode which depends strongly on the size of the Au spot and the size of the p-GaAs electrode. This unexpected behavior is explained in terms of rates of partial reactions, such as anodic Au dissolution and cathodic O_2 reduction, which can occur on different parts of the electrode surface. It is concluded that, in general, the rate of a localized reaction at a semiconductor crystal depends not only on the size of the localized area, but also on the amount of crystal surface area exposed to the electrolyte.

Previously we have shown that Au patterns can be deposited photocathodically on low-doped ($<2 \times 10^{17}/\text{cm}^3$) p-GaAs electrodes in an alkaline $\text{KAu}(\text{CN})_2$ solution with excess CN^- ions (1, 2). Further investigations showed, however, that various unexpected effects were induced by changing either the size of the illuminated area on the p-GaAs electrode or the size of the electrode itself. This paper reports the results of some basic experiments which reveal these size effects. Both the size of an illuminated circular spot and the size of the electrode were varied between wide limits.

The rates of mass-transport-controlled reduction of $\text{Au}(\text{CN})_2^-$ ions and O_2 at illuminated spots on a negatively biased low-doped p-GaAs electrode are considered. It appeared that photocathodically deposited Au spots dissolved slowly when, after illumination, the electrode was left at open circuit in the dark. Obviously, this may represent a serious problem in practical photoselective Au plating. The dissolution behavior of the Au spots is discussed in some detail. In connection with our study on the initiation of selective electroless plating on electrocatalytic patterns (3) we investigated the possibility of electroless gold deposition in the dark on previously photocathodically deposited Au spots. The electroless gold deposition reaction is a heterogeneous autocatalytic reaction in which electrons are transferred from the reducing agent BH_4^- to $\text{Au}(\text{CN})_2^-$ ions under open-circuit conditions (4-6). Okinaka *et al.* have shown that high-density electroless gold patterns with details down to 5 μm can be deposited on a Si substrate which was previously activated by deposition of electrocatalytic Pd patterns (7). Here we will show that there exists a critical size of isolated Au spots below which electroless gold deposition does not occur.

Experimental

Most of the experimental details were the same as those described in Part I (1). Four different aqueous solutions containing 0.2M KOH were used (4). The electroless gold solution operated at 70°C contained 0.2M KBH_4 , $5 \times 10^{-3}\text{M}$ $\text{KAu}(\text{CN})_2$, 0.1M KCN, and 0.2M KOH. The solutions from which either KBH_4 , or $\text{KAu}(\text{CN})_2$, or KBH_4 and $\text{KAu}(\text{CN})_2$ were removed are denoted by $\text{KAu}(\text{CN})_2/\text{KCN}$, KBH_4/KCN , and KCN, respectively. In one experiment Au was photodeposited on a TiO_2 film on glass from an aqueous solution which contained 0.01M KAuCl_4 and 4 volume percent (v/o) CH_3OH . Unless otherwise stated, experiments were carried out at room temperature and no gas was bubbled through the solution. All potentials are quoted *vs.* a saturated calomel electrode (SCE).

A rotating Au disk electrode was obtained by mounting a Au rod (Goodfellow, 99.99% pure) with a diameter (ϕ) of 2 mm in a tubular KEL F holder and subsequent mechani-

cal polishing with emery paper and 0.05 μm alumina. Various disk electrodes were made from a p-GaAs (100) single-crystal wafer with a doping level of $9 \times 10^{16}/\text{cm}^3$. Stationary p-GaAs disk electrodes with a diameter of 2.6 or 8.0 mm were fabricated by mounting a crystal in a Teflon holder containing a rubber O-ring against which the p-GaAs crystal was pressed by a Teflon screw cap. This prevented penetration of the electrolyte to the back side and edges of the crystal at an operating temperature of 70°C. A rotating p-GaAs disk electrode with a diameter of 3.0 mm was obtained by mounting a p-GaAs disk on the end of a brass rod centered in a tubular polymethylmethacrylate holder. The empty space between the disk and the holder was filled with epoxy resin (Araldite). p-GaAs microdisk electrodes with diameters of 500, 100, 30, and 10 μm were fabricated by masking the crystal surface with a Si_3N_4 or SiO_2 film using standard photolithographic techniques. Uniform Si_3N_4 and SiO_2 films with a thickness of 0.2 μm were obtained by plasma deposition from a SiH_4/N_2 gas mixture at 300°C under reduced pressure (0.3 torr) and chemical vapor deposition from a SiH_4/O_2 gas mixture at 400°C under atmospheric pressure, respectively. A uniform positive photoresist layer was subsequently applied by spin-coating. After removal of this layer at illuminated circular spots on the surface, etching of Si_3N_4 and SiO_2 was performed in a buffered 25% HF solution. At room temperature no differences were observed between the measured currents at microdisk electrodes based either on Si_3N_4 or SiO_2 . However, a Si_3N_4 mask was preferred at an operating temperature of 70°C, since pit formation in the masking film did not occur at working times less than 30 min.

The experimental setup for local illumination of a p-GaAs working electrode in the electrochemical cell is shown in Fig. 1. A circular aperture of variable diameter was uniformly illuminated by an expanded Gaussian beam of a Spectra Physics Ar^+ laser ($\lambda = 454.5\text{-}514.5\text{ nm}$). A reduced image (10 \times) of the aperture was projected onto the surface of the p-GaAs electrode by an objective lens. This resulted in a uniform light intensity distribution in projected circular spots with radii (r) between 5 and 250 μm [a Gaussian light intensity distribution would result if the size of the projected laser spot was limited by light diffraction (8)]. In all experiments the light intensity was 1.5 W/cm^2 . The electrode surface was imaged on a monitor by using an Olympus prism binocular microscope with a built-in Philips VK4902 observation camera and a semitransparent mirror. Prior to local illumination of a desired area on the surface, the electrode was properly placed in the image plane of the objective lens. This was done during illumination of the electrode with a white lamp under open-circuit conditions. Figure 2 shows an example of a Au spot with a radius of 5 μm photocathod-

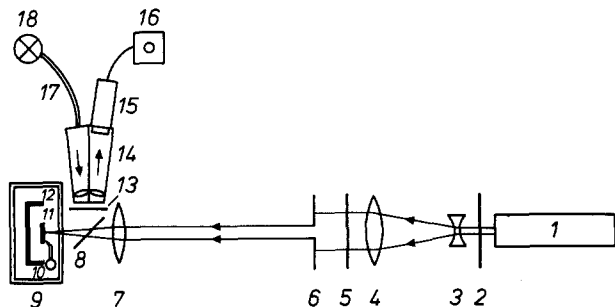


Fig. 1. Top view of experimental setup for projecting a uniformly illuminated circular aperture on a p-GaAs electrode in the electrochemical cell: 1. laser, 2. shutter, 3. diverging lens ($f = -10$ mm), 4. converging lens ($f = 200$ mm), 5. filter, 6. circular aperture, 7. imaging objective lens ($f = 25$ mm), 8. semitransparent mirror, 9. electrochemical cell, 10. SCE electrode with Luggin capillary, 11. p-GaAs electrode, 12. Pt counterelectrode, 13. filter, 14. prism binocular microscope, 15. observation camera, 16. monitor, 17. light cable, and 18. lamp.

ically deposited on a p-GaAs microelectrode with a diameter of $100 \mu\text{m}$.

Results and Discussion

Potentiodynamic behavior of p-GaAs and Au electrodes.—For the sake of comparison with microdisk electrode experiments reported below, Fig. 3 shows some illustrative current-potential curves for p-GaAs (Fig. 3a) and Au (Fig. 3b) disk electrodes. Curve a in Fig. 3a for an illuminated stationary p-GaAs disk electrode in the $\text{KAu}(\text{CN})_2/\text{KCN}$ solution shows the following features when the potential is swept in cathodic direction: an anodic current resulting from GaAs dissolution (9), a diffusion-controlled cathodic current plateau due to two-electron O_2 photoreduction (10), a diffusion-controlled cathodic peak due to photoinitiated Au electrodeposition (1), and the start of H_2 evolution at -1.3V . Curve b in Fig. 3a for an illuminated rotating (500 rpm) p-GaAs disk electrode in the KCN solution shows a well-defined diffusion-controlled cathodic current plateau due to two-electron O_2 photoreduction (10). Finally, curve c in Fig. 3a for a stationary p-GaAs disk electrode in the $\text{KAu}(\text{CN})_2/\text{KCN}$ solution in the dark shows a small cathodic current due to kinetically determined O_2 reduction. A similar curve was ob-

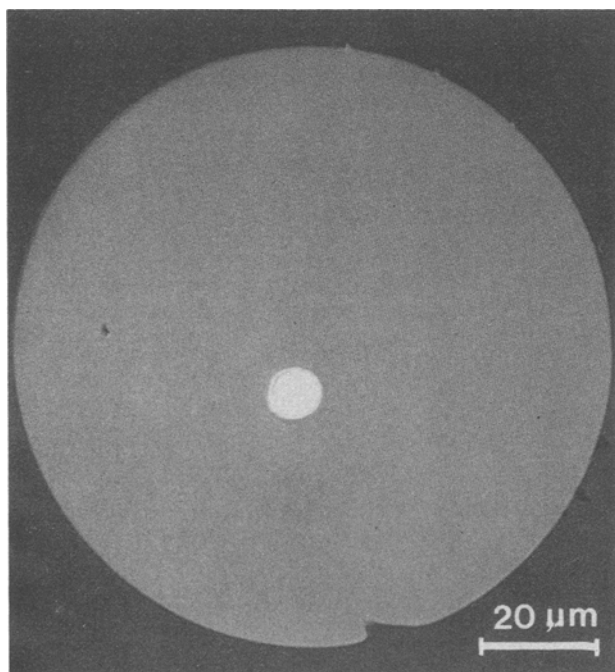
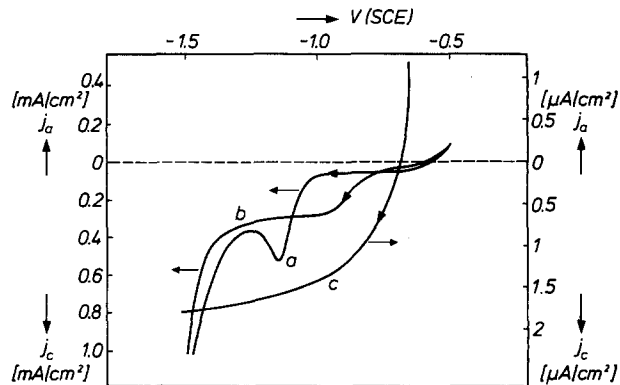
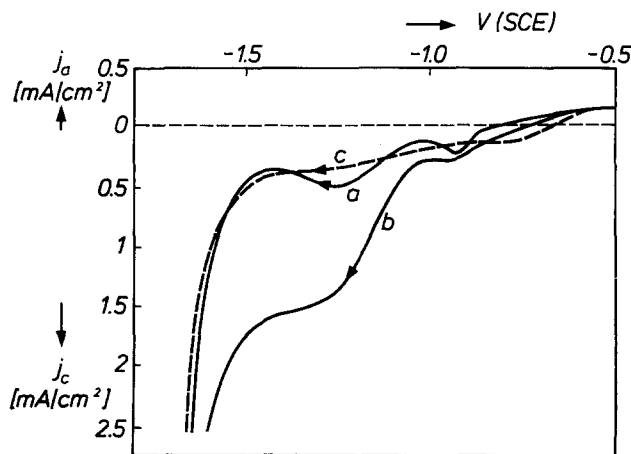


Fig. 2. Interference contrast light microscopy image of a Au spot ($r = 5 \mu\text{m}$) photocathodically deposited on a p-GaAs microelectrode ($\phi = 100 \mu\text{m}$) from the $\text{KAu}(\text{CN})_2/\text{KCN}$ solution at -1.2V for 20s.



a

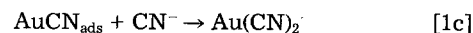
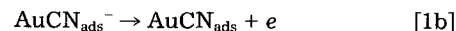


b

Fig. 3. Illustrative current-potential curves of p-GaAs (a) and Au (b) disk electrodes, shown for further reference purposes. Scan rate 10 mV/s . (a) Stationary p-GaAs electrode in $\text{KAu}(\text{CN})_2/\text{KCN}$ solution under uniform illumination (curve a) and in the dark (curve c); rotating (500 rpm) p-GaAs electrode in KCN solution under uniform illumination (curve b). (b) Stationary Au electrode in $\text{KAu}(\text{CN})_2/\text{KCN}$ solution (curve a); rotating (200 rpm) Au electrode in $\text{KAu}(\text{CN})_2/\text{KCN}$ solution (curve b) and in KCN solution (curve c).

tained in the KCN solution. The corresponding current densities differed from one electrode to the other, but they were always smaller than $10 \mu\text{A/cm}^2$. The open-circuit potential of the p-GaAs electrode [$V_{\text{oc}}(\text{GaAs})$] is determined by the rates of anodic GaAs dissolution and cathodic O_2 reduction (10). In the dark $V_{\text{oc}}(\text{GaAs})$ is -0.67V (curve c).

Curves a and b in Fig. 3b show the curves for a stationary and a rotating (200 rpm) Au disk electrode in the $\text{KAu}(\text{CN})_2/\text{KCN}$ solution, respectively. The current at potentials anodic with respect to $\approx -0.9\text{V}$ results from anodic Au dissolution and cathodic O_2 reduction, which take place simultaneously. Anodic Au dissolution was studied in detail by Kirk and Foulkes (11) and occurs according to the following sequence



in which the second step is the rate-determining step. Curve a shows two diffusion-controlled cathodic peaks due to reduction of O_2 and $\text{Au}(\text{CN})_2^-$, respectively. Curve b shows that these peaks changed into plateaus when the electrode was rotated, indicating diffusion-controlled reduction reactions. $\text{Au}(\text{CN})_2^-$ reduction follows the sequence of reactions [1] in reverse (12-14). Curve c for a rotating (200 rpm) Au disk electrode in the KCN solution shows two diffusion-controlled cathodic peaks resulting from two-electron and four-electron O_2 reduction, respec-

tively (15). Curves b and c show that the overpotential for O₂ reduction in the KCN solution is smaller than in the KAu(CN)₂/KCN solution. This can probably be ascribed to increased surface coverage of AuCN_{ads} (reaction [1]).

Light-generated microdisk electrodes.—When the dark current at a semiconductor electrode is negligibly small with respect to the photocurrent, it is possible to confine redox reactions mainly to illuminated areas on the electrode surface (8). Figure 4 shows current transients of a p-GaAs microelectrode with a diameter of 500 μm at -1.2V in the KAu(CN)₂/KCN solution for various radii (r) of an illuminated circular spot. Illumination was started at t = 0. The measured currents (i_c) were converted to current densities (j_c) by the relation j_c = i_c/πr². The current density under illumination is orders of magnitude larger than in the dark (<10 μA/cm²). At the high light intensity used in this experiment, the current maximum, which is characteristic for the initial stages of diffusion-controlled Au deposition (1), is not resolved on the time scale of Fig. 4, since it occurred at times shorter than 50 ms.

The measured current transients are reasonably approximated by the equation for complete mass-transport-controlled reduction reactions at a microdisk electrode with radius r (16)

$$j_c = \sum_i n_i F C_i \left(\left(\frac{D_i}{\pi t} \right)^{1/2} + \frac{4D_i}{\pi r} \right) \quad [2]$$

where n_iF is the molar charge used to reduce the electroactive species i, D_i is the diffusion coefficient, C_i is the concentration, and t is, in the present case, the illumination time. The species i are Au(CN)₂⁻ and O₂ which are simultaneously reduced. The first term in Eq. [2] represents the time-dependent linear diffusion flux (Cottrell equation); the second term represents a steady-state nonlinear (spherical) diffusion flux. Figure 4 shows that for smaller values of r spherical diffusion predominates over linear diffusion at relatively shorter times. A logarithmic plot of the measured steady-state current densities (j_s) vs. r⁻¹ yields a straight line with a slope equal to 0.95, as is shown in Fig. 5 (curve a). This agrees with what is expected from Eq. (2). From the above it follows that, at relatively large illumination time and light intensity, the film thickness of small isolated photoelectrochemically deposited Au spots is roughly proportional to r⁻¹ when a constant deposition time is used. It should be noted, however, that spherical diffusion favors the edges of the spot with respect to the center of the spot. For example, for a spot with r = 65 μm

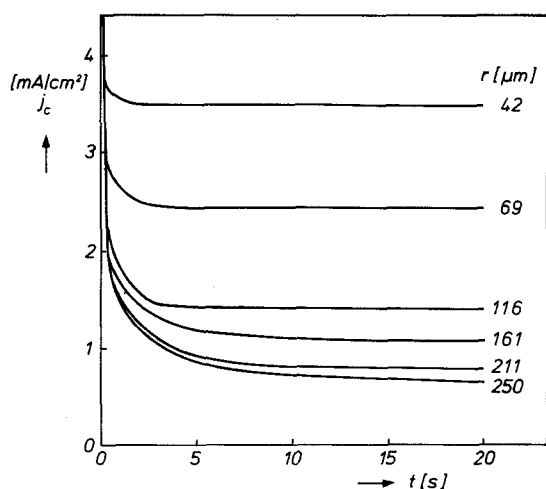


Fig. 4. Potentiostatic current-time transients for complete mass-transport-controlled reduction of Au(CN)₂⁻ and O₂ at light-generated microdisks with various radii (r) on a p-GaAs microelectrode (φ = 500 μm) in the KAu(CN)₂/KCN solution. At t = 0 the potential was stepped from V_{oc} = -0.67V to -1.2V and the light was switched on. The current is initially controlled by linear diffusion and reaches a steady-state value at longer illumination times due to spherical diffusion of reactants to the light-generated microdisk.

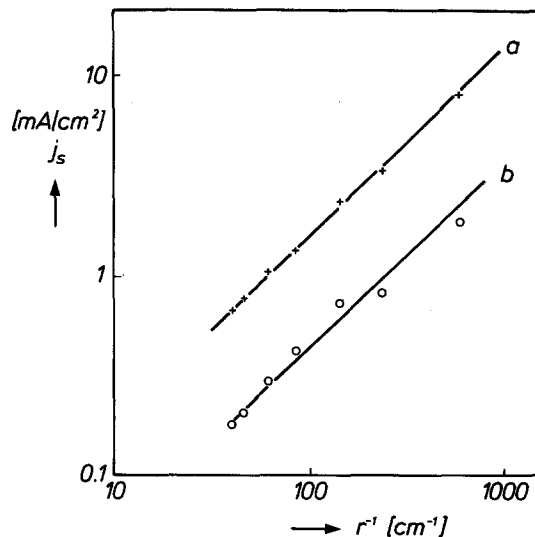


Fig. 5. Logarithmic plot of the steady-state current densities (j_s) vs. the radius (r) of a light-generated microdisk on a p-GaAs microelectrode (φ = 500 μm) at -1.2V. Curve a: KAu(CN)₂/KCN solution, simultaneous reduction of Au(CN)₂⁻ and O₂ (see Fig. 4). Curve b: KCN solution (O₂-saturated), O₂ photoreduction.

the ratio between the steady-state current densities at the edge and at the center equals ≈2.5 (17). This edge effect becomes stronger with increasing spot sizes.

The prolonged reduction of Au(CN)₂⁻ at the light-generated microdisk on the p-GaAs surface results in the deposition of a porous Au spot which starts to behave like a Au microdisk electrode. Consequently, both the reduction of O₂ and Au(CN)₂⁻ proceeding at the Au surface have to be considered. From Fig. 3b (curves b and c) it is expected that at -1.2V the reduction of Au(CN)₂⁻ and O₂ at the Au spot is mainly controlled by diffusion and only slightly by kinetics. As long as light can penetrate through the porous structure of the Au film (18), the potential of the Au spot may be more negative than -1.2V due to a photopotential between Au and p-GaAs (1). Nevertheless, the results of Fig. 4 and 5 (curve a) indicate that a possible kinetic influence on the reduction reactions at the microdisk is extremely small.

For light-generated microdisks on a p-GaAs microelectrode at -1.2V in the KCN solution (O₂-saturated), j_s was also found to be inversely proportional to r, as shown by curve b in Fig. 5. In this case only O₂ was photoreduced under complete diffusion control. This is supported by the fact that O₂ photoreduction at illuminated rotating p-GaAs disk electrodes (10) is diffusion controlled for potentials more negative than -1.0V (Fig. 3a, curve b).

Dissolution of Au spots at open circuit.—The dissolution rate of Au spots in the dark was monitored by measuring open-circuit potential (V_{oc}) transients of the p-GaAs electrode immediately after photocathodic deposition of a single Au spot in the KAu(CN)₂/KCN solution at -1.2V for 20s. Curve a in Fig. 6 shows the transient for a Au spot (r = 250 μm) deposited on a p-GaAs electrode with a diameter of 2.6 mm. The potential was initially near the reversible redox potential V(Au(CN)₂⁻/Au) (≈ -0.89V) and shifted steadily within 150s to the open-circuit potential of the bare p-GaAs electrode (-0.67V). Visual inspection of the electrode at several intermediate times showed that Au dissolution started from the center of the spot. This corresponds with a smaller initial Au film thickness in the center than at the edges of the spot. The Au spot was completely dissolved at t = 150s. Taking the initial amount of consumed cathodic charge used to deposit the Au spot (≈1.4 × 10⁻² C/cm²), this corresponds to an average anodic dissolution rate of ≈0.1 mA/cm². This is of the same order of magnitude as kinetically determined anodic dissolution rates of bulk Au electrodes (11). The same Au spot dissolved more slowly when the oxygen concentration in the solution was decreased, as indicated by curve b in Fig. 6.

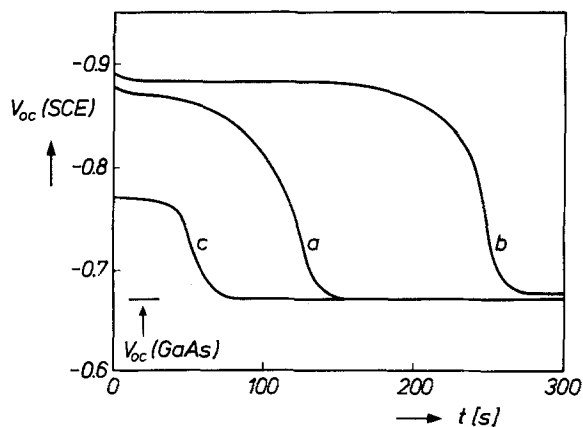


Fig. 6. Open-circuit potential (V_{oc}) transients of a p-GaAs electrode with diameter ϕ in the dark, recorded immediately after mass-transport-controlled photocathodic deposition of a single Au spot ($r = 250 \mu\text{m}$). The Au spot was deposited in the $\text{KAu}(\text{CN})_2/\text{KCN}$ solution at -1.2V for 20s and started to dissolve from $t = 0$. Curve a: $\phi = 2.6 \text{ mm}$, curve b: $\phi = 2.6 \text{ mm}$ with N_2 bubbling, and curve c: $\phi = 8 \text{ mm}$.

On the contrary, the rate of dissolution was increased by O_2 bubbling (not shown). Curve c indicates that the Au spot also dissolved faster when it was deposited on a p-GaAs electrode with a larger diameter (8 mm). As will become clear below, it is important to note that the cathodic dark current densities of the above-mentioned p-GaAs electrodes due to O_2 reduction in the $\text{KAu}(\text{CN})_2/\text{KCN}$ solution were the same.

Figure 7 shows V_{oc} transients of a p-GaAs microelectrode with a diameter of $500 \mu\text{m}$ for various radii of the deposited Au spot. It is observed that at $t = 0$ V_{oc} becomes less negative when the spot size decreases. For all spots V_{oc} became more positive than $V_{oc}(\text{GaAs})$ within a time shorter than 200s. The Au spots turned into rings at intermediate stages of dissolution. The Au rings were only completely dissolved at times longer than 10 min. Only then did V_{oc} reach its final value -0.67V . Similar results were obtained for Au spots deposited on smaller p-GaAs microelectrodes. In some experiments V_{oc} was established at a value close to or more negative than -0.60V for more than 20 min. After this time V_{oc} changed rather abruptly to the final value -0.67V , indicating complete dissolution of the Au spot. The above results indicate that at more anodic potentials the dissolution of Au spots is retarded, as was also found for bulk Au electrodes (11).

The dissolution of Au spots can be described by an electroless corrosion mechanism. The cathodic partial reaction is O_2 reduction which occurs both at the Au spot and the bare p-GaAs surface in the dark (see curves c in Fig. 3). The total cathodic current (i_c) is given by

$$i_c = j_{c,\text{Au}}(\text{O}_2) \cdot A_{\text{Au}} + j_{c,\text{sc}}(\text{O}_2) \cdot A_{\text{sc}} \quad [3]$$

where A_{Au} and A_{sc} are the surface areas of the Au spot and the uncovered p-GaAs surface, respectively. $j_{c,\text{Au}}(\text{O}_2)$ and $j_{c,\text{sc}}(\text{O}_2)$ are the current densities due to O_2 reduction at the Au spot and the p-GaAs surface, respectively. $j_{c,\text{Au}}(\text{O}_2)$ in-

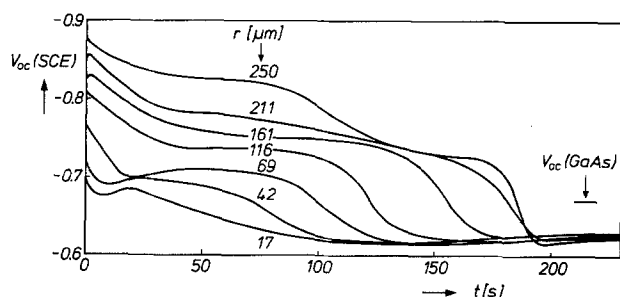


Fig. 7. Similar experiment as in Fig. 6. Au spots with various radii (r) were deposited on a p-GaAs microelectrode ($\phi = 500 \mu\text{m}$).

creases with a decreasing size of the Au spot, due to an enhanced spherical O_2 diffusion flux. This was confirmed by measuring O_2 reduction currents at Au spots on p-GaAs microelectrodes in the $\text{KAu}(\text{CN})_2/\text{KCN}$ solution at a potential corresponding exactly to $V(\text{Au}(\text{CN})_2^-/\text{Au})$ (-0.886V).

For potentials negative of $V_{oc}(\text{GaAs})$ the anodic partial reaction is Au dissolution and the anodic current (i_a) is given by

$$i_a = j_a(\text{Au}) \cdot A_{\text{Au}} \quad [4]$$

where $j_a(\text{Au})$ is the kinetically determined current density due to anodic Au dissolution. For simplicity we neglect the surface roughness of the Au spot. Anodic Au dissolution may be accompanied with anodic GaAs dissolution (9) when the potential becomes more positive than $V_{oc}(\text{GaAs})$.

V_{oc} is the potential at which i_a equals i_c . From Eq. [3] and [4] it follows that for $V_{oc} < V_{oc}(\text{GaAs})$

$$j_a(\text{Au}) = j_{c,\text{Au}}(\text{O}_2) + j_{c,\text{sc}}(\text{O}_2) \frac{A_{\text{sc}}}{A_{\text{Au}}} \quad [5]$$

The right-hand side of this equation will be denoted by the effective cathodic current density $j_c(\text{O}_2)$ at the Au spot. Equation [5] shows that the cathodic current originating from O_2 dark reduction at the bare p-GaAs surface can be regarded as an additional contribution to the O_2 reduction current density at the Au spot. This can be justified by recognizing that holes injected by O_2 at bare GaAs sites can be transferred by conduction in the valence band of p-GaAs to the Au spot where they are consumed in the Au dissolution reaction. Thus, an increase in the value of $j_{c,\text{sc}}(\text{O}_2)$ or A_{sc} has the same effect as an increase in the value of $j_{c,\text{Au}}(\text{O}_2)$.

We now can explain why the dissolution of a Au spot is determined not only by the Au spot itself but also by the p-GaAs electrode. Figure 8 shows schematically the steady-state polarization curves for the partial reactions which may occur during dissolution of a Au spot on a p-GaAs electrode in the $\text{KAu}(\text{CN})_2/\text{KCN}$ solution under open-circuit conditions. The curves are derived from Fig. 3 and literature data (9-11). The dependence of $j_c(\text{O}_2)$ on V_{oc} is depicted for various combinations of the p-GaAs electrode diameter (ϕ) and the Au spot radius (r). $j_c(\text{O}_2)$ increases when ϕ becomes larger or r becomes smaller (Eq. [5]). The indicated sizes are only meant for a qualitative comparison with Fig. 6 and 7. Kirk and Foulkes have shown that the anodic current due to Au dissolution in alkaline cyanide solutions shows Tafel behavior for potentials negative of

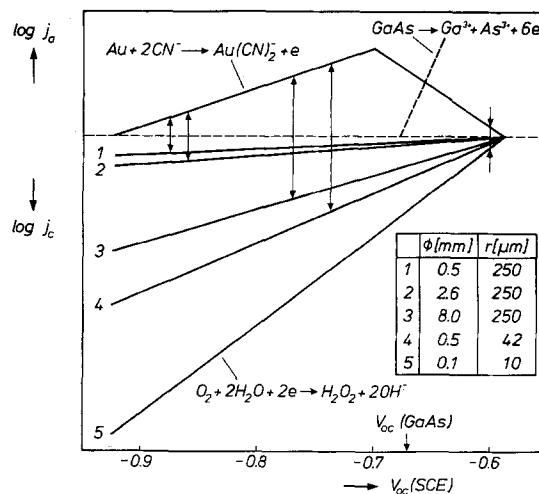


Fig. 8. Schematic semilogarithmic plot of steady-state polarization curves for the partial reactions occurring during dissolution of a Au spot on a p-GaAs electrode at open-circuit conditions in the $\text{KAu}(\text{CN})_2/\text{KCN}$ solution. The effective cathodic current density at the Au spot [$j_c(\text{O}_2)$] increases when the diameter (ϕ) of the p-GaAs electrode increases or the radius (r) of the Au spot decreases. The vertical arrows denote the dissolution rate of the Au spot at the initial open-circuit potential V_{oc} .

$\approx -0.75\text{V}$ (11). The current decrease at more anodic potentials was attributed to an increasing coverage of the Au surface with adsorbed cyanide species (reaction [1]).

From Fig. 8 it is clear that, directly after photocathodic Au deposition at -1.2V , V_{oc} is established at a value positive of $V(\text{Au}(\text{CN})_2^-/\text{Au})$ where Au dissolution starts. The initial V_{oc} is more anodic for a larger p-GaAs electrode or a smaller Au spot. The arrows in Fig. 8 show how this affects the initial dissolution rate of a Au spot. A subsequent shift of V_{oc} originates from a change in the current density of one or more of the partial reactions and vice versa. An evaluation of the resulting time-dependent behavior of V_{oc} during dissolution of a Au spot is beyond the scope of this paper. However, it is, interesting to note that, besides small Au spots, Au rings formed at intermediate stages of dissolution of spots also experience a large nonlinear O_2 diffusion flux. Thus, the formation of Au rings causes V_{oc} to shift in the anodic direction. For small Au spots and Au rings on a p-GaAs microelectrode, V_{oc} is shifted to values considerably more positive than $V_{oc}(\text{GaAs})$, at which further Au dissolution proceeds at a very low rate (11). On larger p-GaAs electrodes, the large anodic current due to GaAs dissolution prevents V_{oc} from becoming as positive with respect to $V_{oc}(\text{GaAs})$.

Possibility of selective electroless gold deposition.—Immediately after photocathodic deposition of a single Au spot on a p-GaAs electrode in the $\text{KAu}(\text{CN})_2/\text{KCN}$ solution at -1.2V for 20s, the electrode was immersed in the electroless gold solution operated at 70°C . It was found that a Au spot deposited on a p-GaAs microelectrode was only intensified by electroless gold deposition when the radius of the spot was $30\ \mu\text{m}$ or larger. Smaller Au spots dissolved completely in the electroless solution. The critical size of Au spots increased drastically with an increasing size of the p-GaAs electrode. For example, for a p-GaAs electrode with a diameter of 8 mm, only Au spots with radii larger than $\approx 200\ \mu\text{m}$ were intensified.

For comparison, Au spots at relatively large mutual distances (5 mm) and with different radii were photodeposited from a $\text{KAuCl}_4/\text{CH}_3\text{OH}$ solution on a TiO_2 film on a glass plate (19). Illumination was carried out with a UV laser for 20s (see Fig. 1). The thin ($<10\ \text{nm}$) TiO_2 film behaves as a dielectric in the dark. Again it was observed that only Au spots with a radius larger than $\approx 30\ \mu\text{m}$ were intensified in the electroless gold solution at 70°C .

The inhibition of electroless gold deposition on small single Au spots will be explained using the concepts of our

originally proposed oxygen-diffusion-size effect (3). More experimental evidence supporting this effect will first be given.

Okinaka has shown that the overall electroless gold deposition reaction on Au electrodes in an oxygen-free electroless solution with a $\text{Au}(\text{CN})_2^-$ concentration larger than 10^{-3}M consists of three partial electrochemical reactions: the oxidation of BH_3OH^- ions formed by hydrolysis of BH_4^- ions, the anodic dissolution of Au, and the reduction of $\text{Au}(\text{CN})_2^-$ ions (5). To explain our results it is necessary to consider O_2 reduction as well. The current densities (j) of the above partial reactions were measured at a Au electrode in the electroless solution and in solutions from which KBH_4 and/or $\text{KAu}(\text{CN})_2$ were absent ("partial" electroless solutions)

$$j_a(\text{BH}_3\text{OH}^-):$$

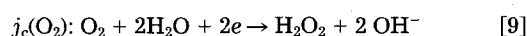
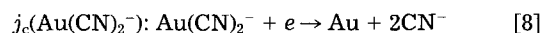
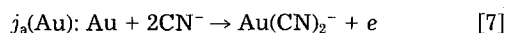
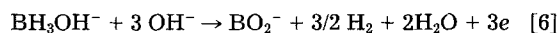


Figure 9a shows current-potential curves for a stationary Au electrode at 70°C in the KCN solution (curve 1), the KBH_4/KCN solution (curve 2), the $\text{KAu}(\text{CN})_2/\text{KCN}$ solution (curve 3), and the electroless solution (curve 4). A stationary p-GaAs electrode, on which a uniform Au film was deposited, showed similar curves. The cathodic current plateau in curve 1 is due to diffusion-limited O_2 reduction. A comparison between curve 1 and Fig. 3b indicates that the anodic current due to Au dissolution is much larger at 70°C than at room temperature. The differences in the current between curves 1 and 2 and between curves 1 and 3 are due to anodic oxidation of BH_3OH^- and cathodic reduction of $\text{Au}(\text{CN})_2^-$, respectively. It was verified that in the complete electroless solution the zero-current potential shown by curve 4 (-0.875V) was the same as the open-circuit potential (V_{oc}) of a Au electrode during electroless gold plating. At V_{oc} the sum of the anodic partial current densities equals the sum of the cathodic partial current densities

$$j_a(\text{BH}_3\text{OH}^-) + j_a(\text{Au}) = j_c(\text{Au}(\text{CN})_2^-) + j_c(\text{O}_2) \quad [10]$$

From Fig. 9a it is seen that at V_{oc} the anodic current density in the KBH_4/KCN solution (curve 2) is larger than the ca-

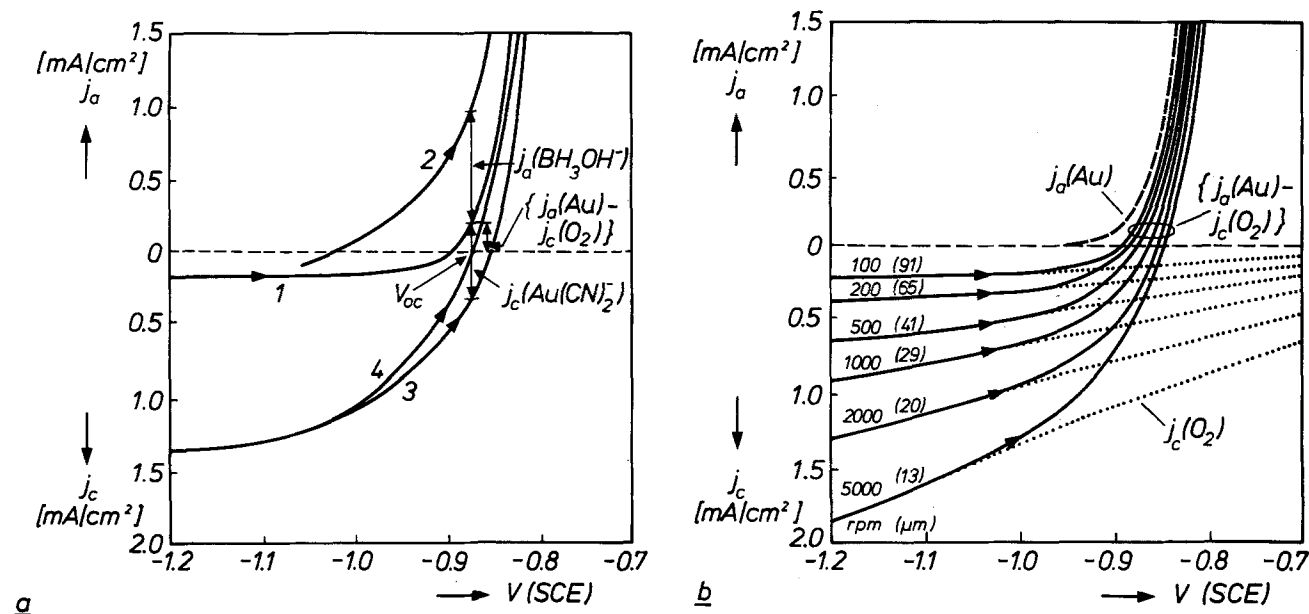


Fig. 9. Current-potential curves for a Au disk electrode ($\phi = 2\ \text{mm}$) at 70°C . Scan rate $10\ \text{mV/s}$. (a) Stationary electrode, curve 1: KCN solution, curve 2: KBH_4/KCN solution, curve 3: $\text{KAu}(\text{CN})_2/\text{KCN}$ solution, and curve 4: complete electroless gold solution. (b) Electrode rotating at various rates (100–5000 rpm) in the KCN solution. The solid lines refer to the measured currents. The dashed and dotted lines represent the estimated partial currents due to anodic Au dissolution and cathodic O_2 reduction, respectively.

thodic current density in the $\text{KAu}(\text{CN})_2/\text{KCN}$ solution (curve 3). A similar discrepancy in oxygen-free solutions was also observed by Okinaka (5). He showed that in the electroless solution $j_a(\text{BH}_3\text{OH}^-)$ was decreased, whereas $j_c(\text{Au}(\text{CN})_2^-)$ remained constant with respect to the corresponding current densities in the "partial" electroless solutions. This interference of BH_3OH^- oxidation with $\text{Au}(\text{CN})_2^-$ reduction was ascribed to the adsorption of $\text{Au}(\text{CN})_2^-$ [AuCN_{ads} species in reaction (1)] on some of the sites where BH_3OH^- would adsorb if the solution did not contain $\text{Au}(\text{CN})_2^-$ (5).

We now consider an isolated Au spot in the electroless solution (still disregarding the substrate surface). The spot acts as a Au microdisk electrode whose V_{oc} is determined by Eq. [10]. At the reversible redox potential $V(\text{Au}(\text{CN})_2^-/\text{Au})$, $j_a(\text{Au})$ equals $j_c(\text{Au}(\text{CN})_2^-)$. From curves 3 and 4 in Fig. 9a it can be deduced that the value of $V(\text{Au}(\text{CN})_2^-/\text{Au})$ at 70°C lies between -0.875 and -0.850V . When V_{oc} is negative of $V(\text{Au}(\text{CN})_2^-/\text{Au})$, electroless gold deposition occurs at a rate corresponding to

$$j_c(\text{Au}(\text{CN})_2^-) - j_a(\text{Au}) = j_a(\text{BH}_3\text{OH}^-) - j_c(\text{O}_2) \quad [11]$$

Electroless Au dissolution occurs when V_{oc} is more positive than $V(\text{Au}(\text{CN})_2^-/\text{Au})$, i.e., when $j_c(\text{O}_2)$ is larger than $j_a(\text{BH}_3\text{OH}^-)$. Thus, the competition between anodic BH_3OH^- oxidation and cathodic O_2 reduction, i.e., the relative values of $j_a(\text{BH}_3\text{OH}^-)$ and $j_c(\text{O}_2)$, will determine whether electroless deposition or electroless dissolution occurs.

The experimental determination of possible effects of an enhanced mass transport of BH_3OH^- and O_2 to small Au spots due to spherical diffusion was simulated by measuring current-potential curves at rotating Au disk electrodes in "partial" electroless solutions at 70°C . It appeared that in the KBH_4/KCN solution $j_a(\text{BH}_3\text{OH}^-)$ was only slightly modified by rotating the electrode, as has also been found by Okinaka (5) and Matsuoka *et al.* (20). This implies that BH_3OH^- oxidation is mainly controlled by kinetics. Consequently, $j_a(\text{BH}_3\text{OH}^-)$ is not noticeably increased when the Au spot becomes smaller. The solid lines in Fig. 9b show the measured current in the KCN solution at various rotation rates. The dashed line shows the estimated partial anodic current due to Au dissolution which is expected to be determined only by kinetics (11, 13). The dotted lines represent the partial cathodic currents due to diffusion-limited O_2 reduction, as they are estimated from measurements at room temperature (cf. curve 3 in Fig. 3b). The numbers in brackets refer to the radius (in μm) of a Au microdisk electrode which collects the same O_2 flux by spherical diffusion as the rotating Au disk electrode does by forced convection (see Appendix).

From a comparison of Fig. 9a and b, it can be understood that in the electroless solution a critical size of the Au spot exists below which $j_c(\text{O}_2)$ is larger than $j_a(\text{BH}_3\text{OH}^-)$. Consequently, V_{oc} will be positive of $V(\text{Au}(\text{CN})_2^-/\text{Au})$ and the Au spot dissolves. An exact prediction of the critical size of isolated Au spots from Fig. 9 is hampered for two reasons. Firstly, in the electroless solution, $\text{Au}(\text{CN})_2^-$ reduction interferes with BH_3OH^- oxidation and O_2 reduction, as noted before. Secondly, the O_2 concentration in the electroless solution is lower than in the KCN solution, since H_2 gas formed by hydrolysis of BH_4^- partially removes O_2 from the solution. Nevertheless, the observed critical size of Au spots on p-GaAs microelectrodes and TiO_2 films in the electroless gold solution can be justified qualitatively by this oxygen-diffusion-size effect (3).

The observed increase of the critical size of the Au spot with an enlargement of the p-GaAs electrode can be ascribed to a collective property of the p-GaAs/Au system, similar to that described in the previous section. From Fig. 9 it is concluded that the increase of the critical spot size results from an effective increase in the cathodic current density at the Au spot due to an additional cathodic current contributed by the bare p-GaAs surfaces (cf. Eq. [5]). Indeed, it was observed that a bare p-GaAs electrode in the electroless solution at 70°C showed a cathodic current density of about $10 \mu\text{A}/\text{cm}^2$ at potentials around -0.875V . Thus, O_2 reduction and BH_3OH^- oxidation, oc-

curing simultaneously at the bare p-GaAs surface, result in a net cathodic current, which further reinforces the oxygen-diffusion-size effect at the Au spot.

Finally, it is expected that photoselectively deposited Au nuclei on a p-GaAs substrate can be intensified by subsequent electroless gold deposition if the density of the patterns is relatively large (7). In this case, the supply of dissolved O_2 in the electroless solution is distributed over a larger gold surface area and consequently, the oxygen-diffusion-size effect may not be noticed anymore.

Conclusions

Cathodically biased low-doped p-GaAs disk electrodes in an alkaline $\text{KAu}(\text{CN})_2$ solution with excess CN^- ions were locally illuminated at a high light intensity by projecting a uniformly illuminated circular aperture onto the electrode surface. The radii of the Au spots formed in this way ranged from 5 to $250 \mu\text{m}$. The rates of photocathodic reduction of $\text{Au}(\text{CN})_2^-$ and O_2 were completely controlled by mass transport to the light-generated microdisk on the p-GaAs electrode. When the projected spot became smaller, the time-dependent linear diffusion flux was more rapidly predominated by a steady-state spherical diffusion flux, which is inversely proportional to the radius of the spot. Consequently, the film thickness of photocathodically deposited Au spots increases when the spot size decreases.

The time-dependent change in the open-circuit potential of p-GaAs electrodes with diameters ranging from $10 \mu\text{m}$ to 8mm was measured in the dark immediately after photocathodic deposition of a single Au spot of variable size. The Au spots dissolved slowly according to an electroless corrosion mechanism. At the open-circuit potential, the anodic current due to Au dissolution is equal to the cathodic current due to O_2 reduction at the Au spot and the uncovered p-GaAs surface. The O_2 reduction current density at the p-GaAs surface is kinetically controlled, while at the Au spot it increases with decreasing spot size due to an enhanced spherical O_2 diffusion flux. Consequently, both the size of the Au spot and of the p-GaAs electrode affect the open-circuit potential and thereby the dissolution rate of the Au spot.

Finally, the possibility of electroless gold deposition at 70°C on a previously photocathodically deposited Au spot in the $\text{KAu}(\text{CN})_2/\text{KCN}$ solution was investigated. Au spots larger than a critical size were intensified by electroless gold deposition, whereas smaller Au spots dissolved completely. The critical size increased drastically when the p-GaAs electrode was enlarged. Measurements of the current densities of the anodic and cathodic partial reactions occurring during electroless gold deposition supported an explanation of these observations in terms of the originally proposed oxygen-diffusion-size effect. Electroless intensification of the Au spot occurs only when the anodic current density, due to kinetically controlled BH_3OH^- oxidation, is larger than the cathodic current density, due to diffusion-controlled O_2 reduction. This effect is reinforced by an additional cathodic current contributed by the uncovered p-GaAs surface.

From this study it can be concluded that, in general, the kinetics of a localized (partial) reaction occurring at a semiconductor crystal may be controlled, not only by the localized area itself, but also by the size of the crystal and its electrochemical activity. In the latter situation, the localized reaction is driven by a counter reaction that proceeds on the entire crystal surface exposed to the electrolyte. This reaction involves majority charge carriers which can move from any part of the crystal surface to the localized area, or vice versa, due to their large diffusion lengths. Using this concept, one can explain, for example, the large rates of localized photoetching of n-GaAs crystals in KOH solutions (22) by accounting for the occurrence of O_2 reduction at the dark areas of the crystal (10).

Acknowledgments

The authors thank Ing. J. M. M. van der Heyden for his contribution to the preparation of p-GaAs microelectrodes and Professor J. J. Kelly (State University of Utrecht) for very helpful discussions.

Manuscript submitted Dec. 2, 1988; revised manuscript received ca. May 5, 1989.

Phillips Research Laboratory assisted in meeting the publication costs of this article.

APPENDIX

The steady-state current densities due to complete mass-transport-controlled O₂ reduction at a stationary Au micro-disk electrode (Eq. [2]) and at a rotating Au disk electrode are given respectively by

$$j_c(\text{O}_2) = \frac{4n_{\text{O}_2}FC_{\text{O}_2}D_{\text{O}_2}}{\pi r} \quad [\text{A-1}]$$

and

$$j_c(\text{O}_2) = 0.62n_{\text{O}_2}FC_{\text{O}_2}D_{\text{O}_2}^{2/3}\nu^{-1/6}\omega^{1/2} \quad [\text{A-2}]$$

where ν is the kinematic viscosity of the solution and ω is the rotation rate. From these equations it follows that the microdisk electrode collects the same O₂ flux as the rotating disk electrode when

$$r = 2.05D_{\text{O}_2}^{1/3}\nu^{1/6}\omega^{-1/2} \quad [\text{A-3}]$$

Using the values $D_{\text{O}_2} = 4.5 \times 10^{-5}$ cm²/s and $\nu = 4.4 \times 10^{-3}$ cm²/s, as given for a 1M KOH solution at 70°C (21), we obtain

$$r = 296\omega^{-1/2} \quad [\text{A-4}]$$

in which r and ω are expressed in μm and rad/s, respectively.

REFERENCES

- J. W. M. Jacobs and J. M. G. Rikken, *This Journal*, **136**, 3633 (1989).
- J. J. Kelly, J. M. G. Rikken, J. W. M. Jacobs, and A. Valster, *J. Vac. Sci. Technol. B*, **6**, 48 (1988).
- J. W. M. Jacobs and J. M. G. Rikken, *This Journal*, **135**, 2822 (1988).
- Y. Okinaka, *Plating*, **57**, 914 (1970).
- Y. Okinaka, *This Journal*, **120**, 739 (1973).
- Y. Okinaka, Abstract 441, p. 632, The Electrochemical Society Extended Abstracts, Vol. 84-2, New Orleans, LA, Oct. 7-12, 1984.
- Y. Okinaka, R. Sard, C. Wolowodiwk, W. H. Craft, and T. F. Retajczyk, *This Journal*, **121**, 56 (1974).
- B. Miller and J. M. Rosamilia, *ibid.*, **132**, 2621 (1985).
- P. H. L. Notten, *Electrochim. Acta*, **32**, 575 (1987).
- J. W. M. Jacobs and J. M. G. Rikken, *J. Electroanal. Chem.*, **258**, 147 (1988).
- D. W. Kirk and F. R. Foulkes, *This Journal*, **127**, 1993 (1980).
- J. A. Harrison and J. Thompson, *J. Electroanal. Chem.*, **40**, 113 (1972).
- E. T. Eisenmann, *This Journal*, **125**, 717 (1978).
- M. Beltowska-Brzenzinska, E. Dutkiewicz, and W. Lawicki, *J. Electroanal. Chem.*, **99**, 341 (1979).
- C. Paliteiro, A. Hamnett, and J. B. Goodenough, *ibid.*, **234**, 193 (1987).
- M. Fleischmann, F. Lassere, J. Robinson, and D. Swan, *ibid.*, **177**, 97 (1984).
- M. Penczek and Z. Strojek, *ibid.*, **227**, 271 (1987).
- Y. Degani, T. T. Sheng, A. Heller, D. E. Aspnes, A. A. Studna, and J. D. Porter, *ibid.*, **228**, 167 (1987).
- J. W. M. Jacobs and C. G. J. M. Nillesen, Submitted to *J. Appl. Phys.*
- M. Matsuoka, S. Imanishi, M. Sahara, and T. Hayashi, *Plat Surf. Finish.*, **75** (5), 102 (1988).
- F. T. B. J. van den Brink, Ph.D. Thesis, Eindhoven University of Technology, p. 76 (1981).
- D. V. Podlesnik, H. H. Gilgen, A. E. Willner, and R. M. Osgood, *J. Opt. Soc. Am. B*, **3**, 775 (1986).

Computation of E_{H} -pH Diagrams for M-S-H₂O Systems: A New Approach

S. M. El-Raghy* and M. F. El-Demerdash*

Department of Metallurgy, Faculty of Engineering Cairo University, Cairo, Egypt

ABSTRACT

A new approach is suggested to establish E_{H} -pH diagrams for M-H₂O and M-S-H₂O systems. Each species is assumed to be the primary product of a reaction between metal, sulfur, or both with water. This primary product is assigned an activity term representing its stability. At any E_{H} -pH level, the species of maximum stability is identified and diagrams are developed by scanning all points (E , pH) at specified resolution. Results of this work are compared with the literature. In some cases, published diagrams are not in agreement either between themselves or with the present study.

Since the introduction of E_{H} -pH diagrams by Pourbaix (1), all methods of drawing these diagrams follow, basically, the same approach to resolve the competing equilibria. All methods consider the general reaction in which species A is converted to B (2), the reaction is



where α , w , b , h , and n are stoichiometric parameters. The reduction electrochemical potential is

$$E_{\text{rev}} = \left(\frac{\Delta F^\circ}{nF} \right) - \left(\frac{2.303RT}{nF} h \right) \text{pH} + \frac{2.303RT}{nF} \log \frac{(a_{\text{B}})^b}{(a_{\text{A}})^\alpha \cdot (a_{\text{H}_2\text{O}})^w} \quad [1]$$

where: ΔF° is the standard free energy change of reaction [1], F is Faraday's constant, R is the gas constant, and T is the absolute temperature.

* Electrochemical Society Active Member.

Reaction [1] associated with E_{H} -pH relation [1] for all possible reaction species is the basis of the main data for all calculation methods. The differences between methods lie in the approach that defines the domains of species stability bordered by these lines.

Linkson *et al.* (3, 4) classified the methods of calculating E_{H} -pH diagrams into three basic approaches: (i) point-by-point, (ii) line elimination, and (iii) convex polygon.

Verhulst and Duby (5) developed a computer method using a point-by-point approach for both M-H₂O and M-S-H₂O systems. For all reactions of the form [1], ΔG is defined such that when its value is negative, the reaction proceeds spontaneously to form species A

$$\Delta G = nF(E - E_{\text{rev}}) \quad [2]$$

where E_{rev} is given by Eq. [1] and E is a given potential. At every point (E , pH), all values of ΔG are calculated and species are excluded according to their ΔG value until a species is assigned as the most stable. The same process is repeated for all points.

Brook (6, 7) considered *a priori* distribution of species according to valency and charge. Any two reactions are as-